THE JOURNAL OF PHYSICAL CHEMISTRY A

Subscriber access provided by King Abdullah University of Science and Technology Library

A: Environmental, Combustion, and Atmospheric Chemistry; Aerosol Processes, Geochemistry, and Astrochemistry

High-Pressure Limit Rate Rules for #-H Isomerization of Hydroperoxyalkylperoxy Radicals

Samah Y Mohamed, Alexander Cory Davis, Mariam J Al Rashidi, and S. Mani Sarathy

J. Phys. Chem. A, **Just Accepted Manuscript** • DOI: 10.1021/acs.jpca.7b11955 • Publication Date (Web): 08 Mar 2018

Downloaded from http://pubs.acs.org on March 13, 2018

Just Accepted

"Just Accepted" manuscripts have been peer-reviewed and accepted for publication. They are posted online prior to technical editing, formatting for publication and author proofing. The American Chemical Society provides "Just Accepted" as a service to the research community to expedite the dissemination of scientific material as soon as possible after acceptance. "Just Accepted" manuscripts appear in full in PDF format accompanied by an HTML abstract. "Just Accepted" manuscripts have been fully peer reviewed, but should not be considered the official version of record. They are citable by the Digital Object Identifier (DOI®). "Just Accepted" is an optional service offered to authors. Therefore, the "Just Accepted" Web site may not include all articles that will be published in the journal. After a manuscript is technically edited and formatted, it will be removed from the "Just Accepted" Web site and published as an ASAP article. Note that technical editing may introduce minor changes to the manuscript text and/or graphics which could affect content, and all legal disclaimers and ethical guidelines that apply to the journal pertain. ACS cannot be held responsible for errors or consequences arising from the use of information contained in these "Just Accepted" manuscripts.

ACS Publications

is published by the American Chemical Society. 1155 Sixteenth Street N.W., Washington, DC 20036

Published by American Chemical Society. Copyright © American Chemical Society. However, no copyright claim is made to original U.S. Government works, or works produced by employees of any Commonwealth realm Crown government in the course of their duties.

High-Pressure Limit Rate Rules for α-H Isomerization of Hydroperoxyalkylperoxy Radicals

Samah Y. Mohamed[1], *Alexander C. Davis*[2,*], *Mariam J. Al Rashidi*[3], *S. Mani Sarathy*[1]

[1] King Abdullah University of Science and Technology, Clean Combustion Research Center, Thuwal, 23955-6900, Saudi Arabia

[2] Franklin and Marshall College, Lancaster, PA, 17604-3003, USA

[3] University of Sharjah, Sharjah, P.O. Box 27272, UAE

ABSTRACT

Hydroperoxyalkylperoxy (OOQOOH) radical isomerization is an important low-temperature chain branching reaction within the mechanism of hydrocarbon oxidation. This isomerization may proceed via the migration of the α-hydrogen to the hydroperoxide group. In this work, a combination of high level composite methods - CBS-QB3, G3 and G4 - is used to determine the high-pressure-limit rate parameters for the title reaction. Rate rules for H-migration reactions proceeding through 5-, 6-, 7- and 8-membered ring transitions states are determined. Migrations from primary, secondary and tertiary carbon sites to the peroxy group are considered. Chirality is

also investigated by considering two diastereomers for reactants and transition states with two chiral centers. This is important since chirality may influence the energy barrier of the reaction as well as the rotational energy barriers of hindered rotors in chemical species and transition states. The effect of chirality and hydrogen bonding interactions in the investigated energies and rate constants is studied. The results show that while the energy difference between two diastereomers ranges from 0.1 - 3.2 kcal/mol, chirality hardly affects the kinetics, except at low temperatures (atmospheric conditions) or when two chiral centers are present in the reactant. Regarding the effects of the peroxy group position and the H-migration ring size, it is found that in most cases, the 1,5 and 1,6 H-migration reactions have similar rates at low temperatures (below ~830K) since the 1,6 H-migration proceeds via a cyclohexane-like transition state similar to that of the 1,5 H-migration.

1. Introduction

Hydrocarbon auto-oxidation chemistry is important in fuel combustion and atmospheric processes [1]. At low temperatures, the oxidation chemistry of hydrocarbon fuels has been detailed previously [2-4] and is shown in Figure 1; it is initiated by H-abstraction from the fuel to form radicals, which undergo a series of O_2 additions (1st and 2nd O_2 additions) and isomerizations that eventually form hydroperoxyalkylperoxy radicals (OOQOOH). OOQOOH can isomerize via the intramolecular migration of a hydrogen atom from the α-carbon to the hydroperoxide group (i.e., α-H isomerization), ultimately leading to a ketohydroperoxide (KHP) and an OH radical. The weak O–OH bond in the ketohydroperoxide then breaks to form OH and a ketoalkoxy radical. This sequence of chain branching reactions is the reason for low-temperature reactivity leading to chemical and thermal runaway. This work focuses on the low temperature oxidation

chemistry of n- [5-6] and iso-alkanes [7-10], which are important components in diesel [11] and gasoline [12] fuels; however, similar pathways are also important in cycloalkanes [13-14].

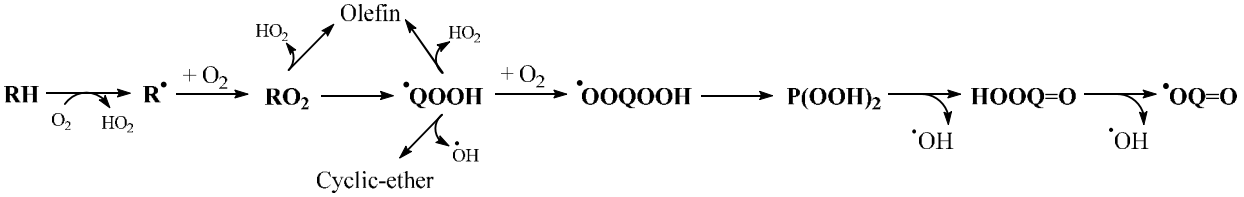

Figure 1. Low temperature oxidation scheme of alkyl radical

OOQOOH radicals are important intermediates in low temperature oxidation chemistry for most conventional fuels [1, 15]. The α-H isomerization reactions of OOQOOH to KHP and hydroxyl radicals have previously been studied [16-20]. However, only Miyoshi [17] considered the rates where the peroxy is positioned at a tertiary site, and none of these studies investigated the effect of chirality on the calculated rates. Previous work has shown that the competition between standard α-H isomerization reactions and alternative isomerizations determines if molecules can undergo extensive auto-oxidation leading to highly oxygenated intermediates [1, 21-24].

Curran et al. [25-26] assigned the rates for the OOQOOH isomerization by analogy to RO_2 isomerization. A correction factor of -3 kcal/mol was added to the activation energy in order to account for the weakness of the C-H bond at the α-site. Moreover, the pre-exponential factor is multiplied by a factor of 0.5 to account for the OOH steric hindrance. However, Sharma et al. [16] calculated the rates of RO_2 and OOQOOH isomerization pathways and showed that the difference in the activation energy between the two channels ranged from 0 to 8.6 kcal/mol for different reactions and thus, the 3 kcal/mol reduction in activation energy was not a valid assumption. Meanwhile, Miyoshi [17] proposed rate rules, calculated at the CBS-QB3 level of theory, for the unimolecular reactions of RO_2, QOOH, and OOQOOH radicals with different possible alkyl substitutions. Miyoshi [17] considered the OOQOOH site specific isomerization

rates based on the nature of both the abstracted hydrogen and the abstracting peroxy group. A recent study by Yao et al. [18] suggested that rate rules calculated based on the minimum-sized representative OOQOOH radical as previously considered [16-17] might be inaccurate, thus, they provided rate rules obtained by averaging the rates of a few representative reactions calculated using a non-standard CBS-QB3 method modified with MP2 for geometry optimization. They calculated the high-pressure-limit and pressure dependent rate rules for both standard and alternative OOQOOH isomerization, where the former abstracts the hydrogen at the α-site to the OOH group, leading to KHP+OH, and the latter abstracts any other hydrogen.

OOQOOH isomerization was also considered by Goldsmith et al. [19] and Asatryan et al. [20], where they studied the potential energy surface of $R+O_2$ and $QOOH+O_2$ for n,i-propyl and 2-pentyl radicals, respectively. They thoroughly discussed the potential energy surface and showed that the OOQOOH isomerization to KHP+OH is the dominant chain branching reaction at low temperatures (below 1000 K) [19-20].

Bugler et al. [27] evaluated the effect of OOQOOH isomerization rate constants calculated by Miyoshi [17] and Sharma et al. [16] on the ignition delay times of pentane isomers. They showed that Sharma's rate coefficients yield better agreement with experimental ignition delay data. Bugler et al. [27] attributed this to the coupled hindered rotor treatment implemented by Sharma et al. [16] in order to account for hydrogen bonding (HB) conformers, which may present in the OOQOOH radicals. However, Davis et al. [28] showed that the HB conformer, in structurally similar hydroxyalkoxy radicals, is not always the most favorable structure, particularly when the destabilizing effect of the ring strain imposed by hydrogen bonding is greater than the stabilizing effect resulting from the hydrogen bond. Chirality further complicates the effect of hydrogen bonding on OOQOOH stability.

For stable molecules with two chiral centers, four diastereomers can be formed, which can be separated into two groups: *mixed* chirality (RS, SR), and *same* chirality (RR, SS). For structures with two or more chiral centers, chirality affects the number and type of dihedral interactions, which in turn can affect the rotational barrier, and therefore the calculated A-factor. Moreover, the gauche/anti interactions between the substituents of the chiral center can affect the barrier heights [29].

In transition states, chirality exists when abstracting from secondary sites of OOQOOH radicals when abstracting from α-site to the OOH group. Additionally, H-migration from a primary carbon (C-OOH) can create a pseudo-chiral center, since abstracting either of the two primary hydrogens yields different axial/equatorial arrangements in the transition state. Chirality in transition states can be described by the configuration of the substituent, or the remaining alkyl chain, which is not involved in the migration ring (alkyl group, hydroperoxide group or hydrogen). For non-planar ring structures, this substituent can either be in the axial or equatorial position relative to the transition state ring, as illustrated in Figure 2.

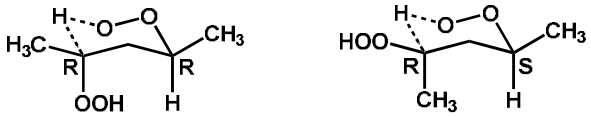

Figure 2. Chirality in transition states

Davis and Francisco [30] showed that chirality can result in as much as a 1.8 kcal/mol difference in activation energies for 1,5 and 1,6 H-migration in alkyl radicals. They also studied in detail [29] the effect of the branched methyl group on the rate coefficients and enthalpies of H-migration reactions for a series of methylalkyl radicals from C3 to C7. They found that for the 1,5 and 1,6 H-migration transition states the barrier for the equatorial configuration was lower than the axial configuration. This is because the axial position of the alkyl group results in gauche interaction

with the transition state ring while the equatorial was anti. The axial configuration destabilized the transition state by 0.8 kcal/mol and resulted in a higher energy barrier.

In their study, Davis and Francisco [29] found that the rates of alkyl isomerization reactions proceed via transition states wherein the alkyl groups in an equatorial position are 2-6 times (and sometimes an order of magnitude) faster than those where the alkyl group is in an axial position. If such differences are not taken into consideration, the rate rule estimates will be inaccurate.

Chirality also has an effect on OOQOOH isomerization; however, this effect has not been previously reported in the literature. In the case of OOQOOH isomerization, the terminal substituent is a hydroperoxide (OOH) group. For isomerization transition states, the axial position of the OOH group may result in HB, which stabilizes the transition state and potentially lowers the barrier. This could lead to faster rates for the axial rather than the equatorial configuration. Therefore, it is important to study the effect of chirality on OOQOOH isomerization.

This work aims to determine the rate parameters for OOQOOH radical isomerization reactions. Detailed conformational analysis is conducted, and the effects of chirality and hydrogen bonding on the calculated rates are assessed. Isomerization via five-, six-, seven- and eight-membered ring transition states, with all possible positions of the peroxy and the H-abstraction sites (primary, secondary or tertiary), are considered and tunneling corrections are applied. The obtained results are compared to the rates available in the literature for similar reactions.

2. Methods

Geometry optimization and frequency calculations of all reactants, products and transition states were performed using the Gaussian09 [31] suite of programs. Two diastereomers were considered for species with two chiral centers: one with mixed chirality (RS or SR), and another

with the same chirality (RR or SS) at both centers. All possible conformations of all species and transition states were determined using the B3LYP/6-31+G(d,p) method. Additional geometry optimizations at the B3YLP/6-311++G(2df,2pd) were carried out for all conformations that are within 0.5 kcal/mol of the minimum conformer. Frequency calculations were carried out at the same level of theory, and a scaling factor of 0.9679 was applied [32]. More accurate energies of the optimized lowest energy conformers were calculated using the CBS-QB3, G3 and G4 composite methods [33-35]. The reported enthalpies of formation are the average of six values calculated at the CBS-QB3, G3 and G4 levels of theory using two sets of isodesmic reactions [36-38] for each species where the auxiliary thermochemistry is adopted from ATcT tables[39] and NIST WebBook[40] (further details in supplementary material). Somers and Simmie [41] reported a two times root mean squared deviation (an approximate 95% confidence interval) of 1.2 kcal/mol, compared to ATcT values, for the average of CBS-QB3, G3 and G4 atomization values for radicals. The use of isodesmic reactions can reasonably be expected to further improve this value. Transition states were confirmed by the presence of a single imaginary frequency corresponding to the reaction path, as well as IRC calculations performed at the B3LYP/6-31+G(d,p) level of theory. The 1D hindered rotor treatment was applied using the Pitzer and Gwinn method [42]. Relaxed scans in 10^{o} increments of all hindered rotors were calculated at the B3LYP/6-31+G(d,p) level of theory (further details in supplementary material). Tunneling corrections were included using the Eckart method and barrier width values from IRC calculations. Rate parameters were determined using classical transition state theory (CTST), which overestimates rate constants compared to variational transition state theory (VTST) [43]. The latter is up to three times more accurate at high temperatures (1000-1500K) [44-45]. However, VTST is computationally expensive for the relatively large systems considered in this study, and

the OOQOOH isomerization reaction is more prone to occur at low temperatures (below 900K). Therefore, we used CTST, as implemented in ChemRate [46]. The optimized geometries and scaled frequencies calculated at the B3YLP/6-311++G(2df,2pd) were used as input for ChemRate, along with the averaged energies (averages of values calculated at the CBS-QB3,G3, and G4 levels of theory). The rotational energy barriers for every hindered rotor were also used as input for ChemRate. These values, along with the Eckart tunneling factors, were obtained from calculations conducted at the B3LYP/6-31+G(d,p) level of theory. The resulting rates were fit to a three parameter modified Arrhenius equation over the temperature range of 300-1500 K. These calculations were performed for the species shown in Figure 3.

Hydrogen migration can be described as *a,b* H-migration, where *a* is the location of the migrated hydrogen and *b* is the location of the abstracting peroxy radical. Alternatively, the migration can be described as N*CD*, where N is the number of components or atoms in the transition state ring, including the hydrogen. *C* and *D* represent the chemical nature (P = primary, S = secondary, and T = tertiary) of the carbon sites of the OOH and OO group, respectively. R and S subscripts will be added to the *C* and/or *D* to indicate the chiral nature of the carbon sites. Where applicable, transition state chirality will also be indicated by the superscript A or E to signify axial or equatorial substitution, respectively. Both the *a,b* H-migration and N*CD* notations will be used to highlight different aspects of the reactions.

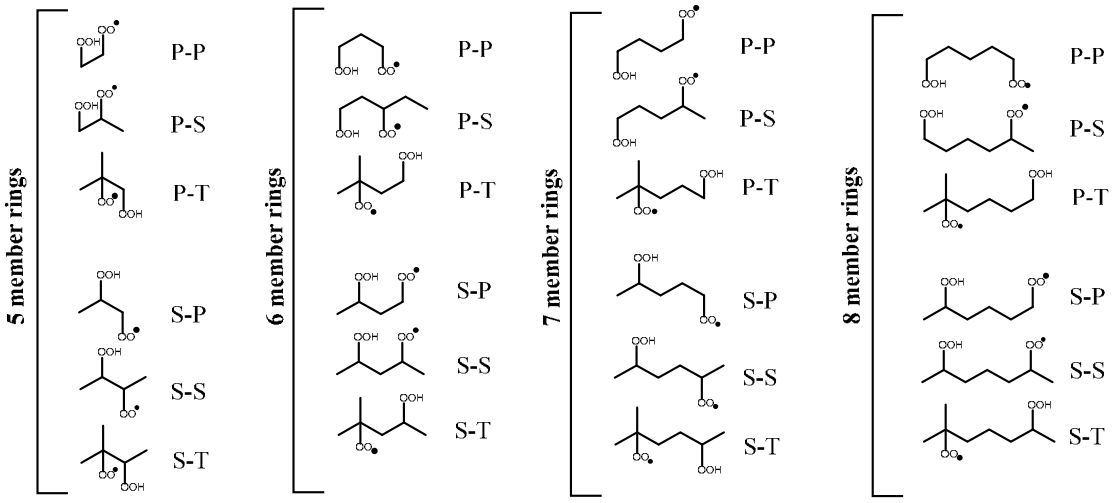

Figure 3. Representative molecules investigated in this study for rate calculations

3. Results and discussion

3.1 Lowest energy conformers:

The most stable conformers of reactants, transition states and products for hydroperoxyalkylperoxy reactions must be selected carefully due to the presence of the oxygenated sites that might introduce HB interactions. The minimum energy conformers were explored by rotating all dihedrals of the molecule by 120^{o} at the same time, which leads to 3^{n} conformers, where n is the number of rotors. For transition states where less rotors are available, smaller increments were used for the C-OOH and O-OH bonds (eg. 60^{o}) to capture different possibilities of HB or NHB conformers. The effect of chirality in the minimum energy conformer was also investigated. In this section, the energy values reported to compare HB and NHB structures are calculated at the B3YLP/6-311++G(2df,2pd) level of theory while the values of the heat of formation of axial and equatorial transition states are calculated using an average of isodesmic reactions for energies calculated at the CBS-QB3/G3/G4 composite methods.

For the reactant of 5*CD,* where the oxygenated sites are in alpha positions to each other and either *C* or *D* is on a primary carbon, the molecule forms HB where the hydrogen in the

hydroperoxide group interacts with an oxygen in the peroxy group and stabilizes the molecule. Previous studies reported that decreases in energy resulting from HB can range from 1.5-4 kcal [28, 47]. The effect of this energy stabilization on the kinetics will be discussed in a separate study.

N*SS* reactants have two chiral centers, resulting in four different stereoisomers (RR, RS, SR and SS). Due to symmetry, the conformer and its mirror image (RR and SS) or (RS and SR) have the same kinetic and thermodynamic properties. Therefore, the most stable diastereomers were used: one with mixed chirality (RS or SR) and the other with the same chirality (RR or SS) at both centers. In the text to follow, the terms *mixed* and *same* chirality will refer to RS (or SR) and RR (or SS) conformers, respectively. In 5*SS* the mixed chirality diasteriomer, $5S_SS_R$, forms HB, while the same chirality diastereomer, $5S_RS_R$ does not, as seen in Figure 4,a and 4.b. The HB conformer of $5S_RS_R$ (Figure 4,b) is 0.1 kcal/mol less stable than the NHB conformer. For reactants with one chiral center, such as 5*ST*, each conformer is a mirror image of its stereoisomer. 5*ST* favors the NHB conformer, which is only 0.1 kcal/mol more stable than its HB counterpart.

As the oxygenated sites *C* and *D* are further separated (e.g. beta, gamma or delta to each other), there is a rising steric cost for forming HB ring structures, due to the increasing number of gauche interactions inside the ring. The energy cost of this steric effect may be greater than the stabilizing effect of the HB, resulting in lower energy for the NHB conformer, except in the case of $6S_RS_S$ and 6*PT* as in Figure 4,c and 4,d.

HB is the most stable conformer for the products when the carbonyl and the hydroperoxide groups are alpha, beta, gamma and delta position relative to each other. Special cases are 5*ST*, 6*PP*, 6*SP*, and 6SS where the NHB is the most stable structure by 1.6, 2.4, 1.0 and 2.4 kcal/mol, respectively. The HB conformer of the 5*ST* comprises two alkyl gauche interactions compared to

one gauche interaction for the NHB, making the latter more favorable. For 6*PP* and 6*SP*, primary OOH prefers to be in anti instead of gauche position in the HB conformer. In 6*SS,* the HB structure is less favorable due to the high steric effect resulting from the gauche interaction between C1 and C4, which makes the NHB structure, where C1 and C4 are in the anti position the most stable conformer, as seen in Figure 4,e and 4,f.

As mentioned previously, all transition states contain at least one chiral center. Both diastereomers (R and S/mixed and same chirality) are considered. Chirality in the transition states will be differentiated by whether the terminal chain, or substituents (which are not involved in the transition state), are axial $N^{A}CD$, or equatorial $N^{E}CD$, to the transition state ring structure. In 1,4 H-migration, the cyclopentane transition state structure is close to planar and less puckered, which makes chirality less defined by axial and equatorial configuration. For $5^{E}CD$, the OOH is sterically unable to form HB. In $5^{A}SP$, $5^{A}SS$ and $5^{A}ST$, where the C-OOH is a secondary carbon, HB conformers are lower in energy than the NHB ones, while in primary C-OOH ($5^{A}PP$, $5^{A}PS$, $5^{A}PT$), the OOH group is not sufficiently axial to form an HB conformer. This is because the co-substituent (hydrogen) is not strong enough to push the OOH to a full axial position; therefore the NHB conformer is more stable.

For $N^{A}CD$ and $N^{E}CD$, where N=6 and 7, the NHB is the minimum energy conformer. In $N^{A}CD$, the high strain imposed by bringing the OOH and the OO groups close enough to form HB, as well as the great distance between the H and O (3-3.7 Å) makes NHB the more stable conformer. On the other hand, $8^{A}CD$ transition states tend to form HB conformers that comprise a flexible cycloheptane-like ring, in which the C-H..O angle is approximately 180^{O} where H is the migrating hydrogen, as shown in Figure 4,g. The flexibility of the cycloheptane ring structure overcomes its high ring strain and favors the HB structure [28].

In terms of chirality, Table 1 shows that the difference in heat of formation between the diastereomers of 1,4 and 1,5 H-migration ranges from 0.1 to 0.9 kcal/mol. This difference increases up to 1.7 and 2.8 kcal/mol for 1,6 and 1,7 H-migration, respectively. Negative values indicate that the axial substituent (OOH group) is more stable than the equatorial conformer. In most cases, where the axial forms a HB, the axial is expected to be more stable. Exceptions are the 5*PP,* 5*PS*, 5*PT*, 7*PS* and 8*PS*, where the axial primary OOH group is unable to form HB, making the equatorial a more stable conformer. In 8*SS*, the mixed and same chirality transition states are $8S_RS_S$ and $8S_RS_R$, where the OOH group is in axial configuration (R) in both transition states. Therefore, the most stable conformer in this case, will be determined based on the chiral nature of the peroxy site, or the configuration (axial or equatorial) of the CH_3 substituent. In $8S_RS_S$, the terminal CH_3 is axial to the transition state, forming a gauche interaction with the remaining alkyl chain and destabilizing the transition state, while the terminal CH_3 in $8S_RS_R$ is equatorial and in an anti-position to the transition state backbone, which makes the equatorial $8S_RS_R$ more stable. In 5*SS*, the $5^{E}SS$ is the more stable conformer due to the less strained transition state ring, in addition to the absence of the gauche interaction between the peroxy and the hydroperoxide groups compared to $5^{A}SS$. The effect of this difference in the rate constant is discussed in a subsequent section (3.3.4).

a) $5S_RS_R$, minimum NHB conformer

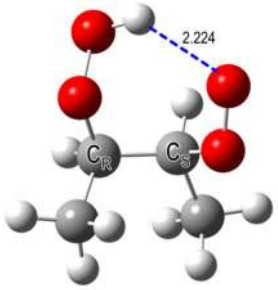

b) $5S_RS_S$, HB conformer

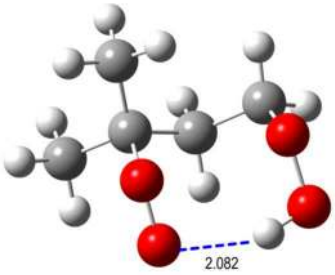

c) 6*PT*, minimum HB conformer

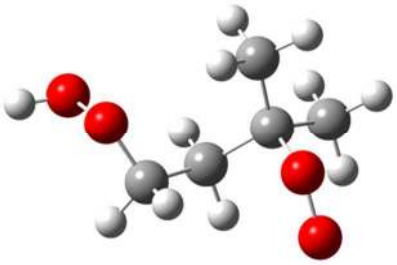

d) 6*PT*, NHB conformer

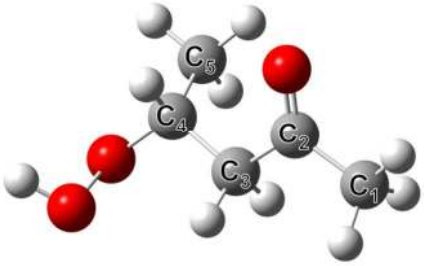

e) 6*SS*, minimum NHB conformer

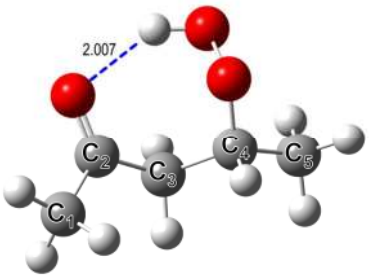

f) 6*SS*, HB conformer

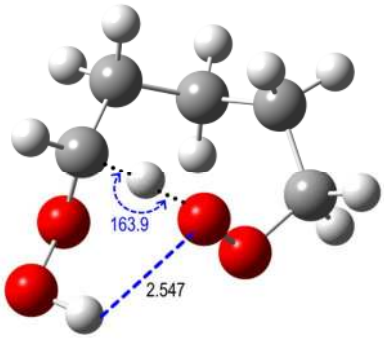

g) 8^{A}*PP*, HB conformer

Figure 4. Minimum energy conformers and their hydrogen bonding counterparts. Values represent distances in Angstroms or angles in degrees.

Table 1. Energy difference (kcal/mol) between mixed and same chirality in transition states, or axial and equatorial configurations at 298 K.

Ring size	OOH	OO.	Formula			$\Delta H=(Hf^{A}-Hf^{E})$
5 membered ring	P	P	HOOCH2CH2OO	$5P_RP$ [1]	A	0.1
				$5P_SP$	E	
	P	S	HOOCH2CH(CH3)OO	$5P_RS_R$	A	0.8
				$5P_SS_R$	E	
	P	T	HOOCH2C(CH3)(CH3)OO	$5P_RT$	A	0.9
				$5P_ST$	E	
	S	P	HOOCH(CH3)CH2OO	$5S_SP$	A	-0.4
				$5S_RP$	E	
	S	S	HOOCH(CH3)CH(CH3)OO	$5S_SS_R$	A	0.7
				$5S_RS_R$	E	
	S	T	HOOCH(CH3)C(CH3)(CH3)OO	$5S_ST$	A	-0.4
				$5S_RT$	E	
6 membered ring	P	P	HOOCH2CH2CH2OO	$6P_RP$	A	-0.7
				$6P_SP$	E	
	P	S	HOOCH2CH2CH(C2H5)OO	$6P_RS_S$	A	-0.8
				$6P_SS_S$	E	
	P	T	HOOCH2CH2C(CH3)(CH3)OO	$6P_RT$	A	-0.6
				$6P_ST$	E	
	S	P	HOOCH(CH3)CH2CH2OO	$6S_RP$	A	-0.6
				$6S_SP$	E	
	S	S	HOOCH(CH3)CH2CH(CH3)OO	$6S_SS_S$	A	-0.8
				$6S_RS_S$	E	
	S	T	HOOCH(CH3)CH2C (CH3)(CH3)OO	$6S_ST$	A	-0.6
				$6S_RT$	E	
7 membered ring	P	P	HOO(CH2)4OO	$7P_SP$	A	-1.0

				$7P_RP$	E	
	P	S	HOO(CH2)3CH(CH3)OO	$7P_RS_S$	A	1.1
				$7P_SS_S$	E	
	P	T	HOO(CH2)3C(CH3)(CH3)OO	$7P_ST$	A	-1.1
				$7P_RT$	E	
	S	P	HOOCH(CH3)(CH2)3OO	$7S_RP$	A	-1.7
				$7S_SP$	E	
	S	S	HOOCH(CH3)(CH2)2CH(CH3)OO	$7S_RS_S$	A	-1.7
				$7S_SS_S$	E	
	S	T	HOOCH(CH3)(CH2)2C(CH3)(CH3)OO	$7S_RT$	A	-1.7
				$7S_ST$	E	
8 membered ring	P	P	HOO(CH2)5OO	$8P_SP$	A	-2.8
				$8P_RP$	E	
	P	S	HOO(CH2)4CH(CH3)OO	$8P_SS_R$	A [2]	0.1
				$8P_SS_S$	E [2]	
	P	T	HOO(CH2)4C(CH3)(CH3)OO	$8P_ST$	A	-2.8
				$8P_RT$	E	
	S	P	HOOCH(CH3)(CH2)4OO	$8S_RP$	A	-2.9
				$8S_SP$	E	
	S	S	HOOCH(CH3)(CH2)3CH(CH3)OO	$8S_RS_S$	A	0.1
				$8S_RS_R$	E	
	S	T	HOOCH(CH3)(CH2)3C(CH3)(CH3)OO	$8S_RT$	A	-3.3
				$8S_ST$	E	

[1] In N*PD*, primary C-OOH is not a chiral center. R and S reflect the chirality of the transition state where two migrated hydrogens are distinguishable, resulting in a pseudo chiral center at the primary site.

2 A and E refer to a methyl group substituent of C-OO.

3.2 Energy calculations

The reported energies are averages of the values calculated using CBS-QB3, G3 and G4 methods, as recommended by Somers and Simmie [41]. Table 2 summarizes the energy barriers, $\Delta H^{\ddagger}$, of the investigated reactions. The enthalpies of formation of all species and transition states are estimated using an average of two sets of isodesmic reactions, as detailed in Supplementary Material. Somers and Simmie [41] showed that the CBS-QB3 and G3 methods tend to underestimate the enthalpy of formation compared to experimental values with a wider error distribution for the former; whereas G4 overestimates the predicted values compared to the experimental values. They showed that averaging the three methods results in better agreement with the experimental values. Table 2 shows that CBS-QB3 underestimated the energy compared to the averaged value, where G3 and G4 methods overestimated the enthalpy and the barrier.

Table 2 shows that the energy barriers of the investigated reactions decrease with increasing ring size. The 1,4 H-migration proceeds via a strained cyclopentane-like ring, which leads to a high energy barrier. The seven-member ring transition state of the 1,6 H-migration is expected to be higher in energy than that of the 1,5 H-migration, due to higher ring strain. However, the two values are similar, with the energy barrier of 1,6 H-migration being slightly lower than that of 1,5 H-migration. This is because the migrating hydrogen in the 1,6 H-migration is located between the abstracting oxygen and the abstraction carbon site (C-H..O~180^{o}), which leads to a cyclohexane-like transition state. For the 1,7 H-migration, as mentioned earlier, the flexibility of the cycloheptane-like transition state ring allows for rearrangement to lower energy conformers. This flexibility will result in a more stable transition state due to the induced HB interaction and therefore, a low barrier for the 1,7 H-migration.

Table 2. Reaction barriers ($\Delta H^{\ddagger}$) calculated at CBS-QB3, G3, G4 and the averaged value.

Ring size	OOH	OO.	Formula	ΔH‡ (kcal/mol)			
				CBS-QB3 [1]	G3 [1]	G4 [1]	average [2]
5 membered ring	P	P	HOOCH2CH2OO	30.9	33.2	32.4	32.1
	P	S	HOOCH2CH(CH3)OO	30.5	32.8	31.9	31.7
	P	T	HOOCH2C(CH3)(CH3)OO	28.5	30.9	30.3	29.9
	S	P	HOOCH(CH3)CH2OO	28.0	30.4	30.6	29.7
	S	S	HOOCH(CH3)CH(CH3)OO	26.4	29.0	28.7	28.0
	S	T	HOOCH(CH3)C(CH3)(CH3)OO	26.1	28.4	28.3	27.6
6 membered ring	P	P	HOOCH2CH2CH2OO	19.3	21.8	21.6	20.9
	P	S	HOOCH2CH2CH(C2H5)OO	19.8	22.3	21.8	21.3
	P	T	HOOCH2CH2C(CH3)(CH3)OO	20.8	23.0	22.7	22.2
	S	P	HOOCH(CH3)CH2CH2OO	18.1	20.1	20.6	19.6
	S	S	HOOCH(CH3)CH2CH(CH3)OO	17.7	20.2	20.1	19.3
	S	T	HOOCH(CH3)CH2C (CH3)(CH3)OO	18.0	20.6	20.7	19.8
7 membered ring	P	P	HOO(CH2)4OO	17.9	20.0	20.1	19.3
	P	S	HOO(CH2)3CH(CH3)OO	18.4	20.4	20.5	19.8
	P	T	HOO(CH2)3C(CH3)(CH3)OO	19.4	21.4	21.4	20.7
	S	P	HOOCH(CH3)(CH2)3OO	15.5	17.7	18.1	17.1
	S	S	HOOCH(CH3)(CH2)2CH(CH3)OO	15.9	18.0	18.5	17.4
	S	T	HOOCH(CH3)(CH2)2C(CH3)(CH3)OO	17.1	19.1	19.5	18.6
8 membered ring	P	P	HOO(CH2)5OO	17.1	19.1	19.5	18.6
	P	S	HOO(CH2)4CH(CH3)OO	15.9	17.7	18.6	17.4
	P	T	HOO(CH2)4C(CH3)(CH3)OO	17.1	19.0	19.4	18.5
	S	P	HOOCH(CH3)(CH2)4OO	14.5	16.4	17.3	16.1
	S	S	HOOCH(CH3)(CH2)3CH(CH3)OO	13.3	15.2	16.3	14.9
	S	T	HOOCH(CH3)(CH2)3C(CH3)(CH3)OO	14.9	16.8	17.6	16.4

[1]Average of two values

[2]Average of six values

3.3 High pressure rate rules:

3.3.1 Rate constants of OOQOOH isomerization to KHP+OH

High pressure limit rate constants are fitted to the single modified Arrhenius equation, over the temperature range of 300–1500 K, using the transition state theory

$$k(T) = \kappa(T) A T^n e^{-E_a/RT}$$

where A is the frequency factor, n is the temperature fitting parameter, T is temperature, E_a is the activation energy and $\kappa(T)$ is the transmission coefficient used to correct for tunneling. The frequency factor A, is an indication of the entropic difference between the transition state and the reactant $\Delta S^{\ddagger}$. The rate constants are calculated for a minimum-sized representative reaction, and are detailed in Table 3 on a per hydrogen basis.

Table 3. High pressure limit rate parameters for OOQOOH ismoerization reaction fit between 300 K and 1500 K, per hydrogen basis.

				Modified Arrhenius Parameters		
Ring size	**OOH**	**OO.**	**Reactant**	**Log A**	**n**	**Ea[1]**
5 membered ring	P	P	HOOCH2CH2OO	-4.79	5.07	22.8
	P	S	HOOCH2CH(CH3)OO [2]	-3.79	5.02	22.3
	P	T	HOOCH2C(CH3)(CH3)OO	-4.06	4.90	20.4
	S	P	HOOCH(CH3)CH2OO	-2.97	4.56	20.9
	S	S	HOOCH(CH3)CH(CH3)OO [2]	-0.26	3.92	20.3
	S	T	HOOCH(CH3)C(CH3)(CH3)OO	-0.28	3.73	20.5
6 membered ring	P	P	HOOCH2CH2CH2OO	0.21	3.30	15.0
	P	S	HOOCH2CH2CH(C2H5)OO [2]	1.69	2.98	15.6
	P	T	HOOCH2CH2C(CH3)(CH3)OO	-1.13	3.94	14.1
	S	P	HOOCH(CH3)CH2CH2OO	1.13	3.15	14.2
	S	S	HOOCH(CH3)CH2CH(CH3)OO [2]	2.67	2.80	14.1

	S	T	HOOCH(CH3)CH2C (CH3)(CH3)OO	3.82	2.44	14.9
7 membered ring	P	P	HOO(CH2)4OO	-0.23	3.12	13.2
	P	S	HOO(CH2)3CH(CH3)OO [2]	1.50	2.77	14.3
	P	T	HOO(CH2)3C(CH3)(CH3)OO	3.40	2.47	15.5
	S	P	HOOCH(CH3)(CH2)3OO	0.80	3.06	11.2
	S	S	HOOCH(CH3)(CH2)2CH(CH3)OO [2]	0.55	3.24	11.4
	S	T	HOOCH(CH3)(CH2)2C(CH3)(CH3)OO	2.77	2.60	13.0
8 membered ring	P	P	HOO(CH2)5OO	-0.43	2.90	12.2
	P	S	HOO(CH2)4CH(CH3)OO [2]	1.14	2.65	12.5
	P	T	HOO(CH2)4C(CH3)(CH3)OO	1.79	2.40	12.4
	S	P	HOOCH(CH3)(CH2)4OO	0.81	2.68	10.4
	S	S	HOOCH(CH3)(CH2)3CH(CH3)OO [2]	2.62	2.39	11.0
	S	T	HOOCH(CH3)(CH2)3C(CH3)(CH3)OO	1.70	2.60	10.4

[1] E_a is in kcal/mol

[2] The rates are an average of the rates with same and mixed chirality of the transition states (N-PS/N-SS) and reactant (N-SS). The mixed and same chirality rates are detailed in the Supplementary Material.

3.3.2 Effect of the transition state ring size:

The temperature dependence of the calculated rate constants is shown in Figure 5. Although the barrier heights of 1,5 H-migration are greater than or equal to the those of 1,6 H-migration, as shown in Table 1, the rate constants of these reactions do not always follow the same trend. This indicates the importance of the A-factor or the entropic term, which is a function of the number of rigid rotors in the transition state ring. The rate constants of 1,5 H-migration reactions are almost of the same magnitude or slightly lower than their 1,6 H-migration counterparts. As mentioned earlier, both six- and seven-member rings proceed via a cyclohexane-like transition state ring, and thus, they have similar rate constants. However, at high temperatures, six-

membered ring reactions are faster than its seven-membered ring counterpart, due to the fact that more rotors are locked to form the seven-membered ring transition state, which reduces the entropy and thus, the A-factor for the seven-membered ring reaction. 1,4 H-migration reactions proceeds via the slowest rates due to the relatively high ring strain in the corresponding five-membered ring transition states. Moreover, the rate constants of 1,4 H-migration exhibit stronger temperature dependence than either 1,5 or 1,6 H-migration. The rates for 1,7 H-migration are slower than the 1,5 and 1,6 H-migration, although they have the lowest barrier. This is likely due to the 1,7 H-migrations tying up more rotors in their eight-member ring transition states.

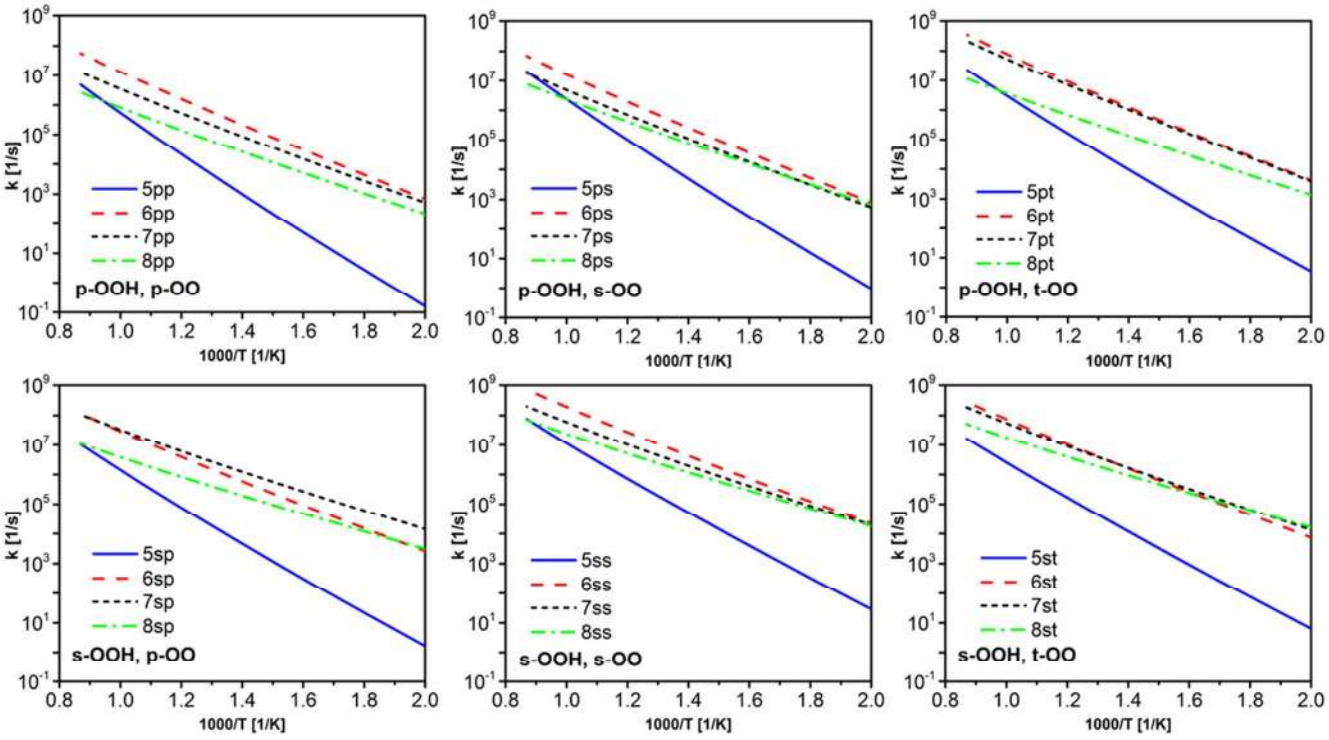

Figure 5. Effect of transition states ring size on calculated rate constants. The legend in each plot follows the N*CD* nomeclature, where N is the ring size, *C* and *D* are the type of the C-OOH and C-OO$^{\cdot}$, respectively.

3.3.3 Effect of the peroxy position

The kinetics of H-migration in OOQOOH depend on the chemical nature of the abstraction site (H being abstracted from primary or secondary carbon) as well as that of the peroxy group. Moreover, the stability of the transition states depends on the substituents at both reacting carbon centers that may introduce gauche interactions. Figure 6 shows the effect of different peroxy position where it can be *P*, *S* or *T*. When the peroxy group is in a primary site (Blue solid lines), the rates are generally up to an order of magnitude slower due to the absence of gauche interactions in the reactant molecules, which renders them more stable. When the peroxy group is in a secondary or tertiary position, the rates depend on the chemical nature of the OOH site. For example, 6*PT* is faster than 6*PS*; although the reaction barrier of the latter is 0.9 kcal/mol lower. This is attributed to the HB nature of the 6*PT* reactant, which increases the rotational barrier and the entropy, thus yielding faster rates for 6*PT* relative to 6*PS*. On the other hand, 5*SS* is faster than *5ST*. This refers to the two gauche interactions present between the terminals for *5ST,* compared to zero or one gauche interaction in 5*SS*. These gauche interactions alter the rotational barrier which affects the A-factor. The directionality of the substituents in the transition state also affects the A-factor, where axial and equatorial result in different interactions and rotational hindrance. This will be discussed in more detail in the section that follows.

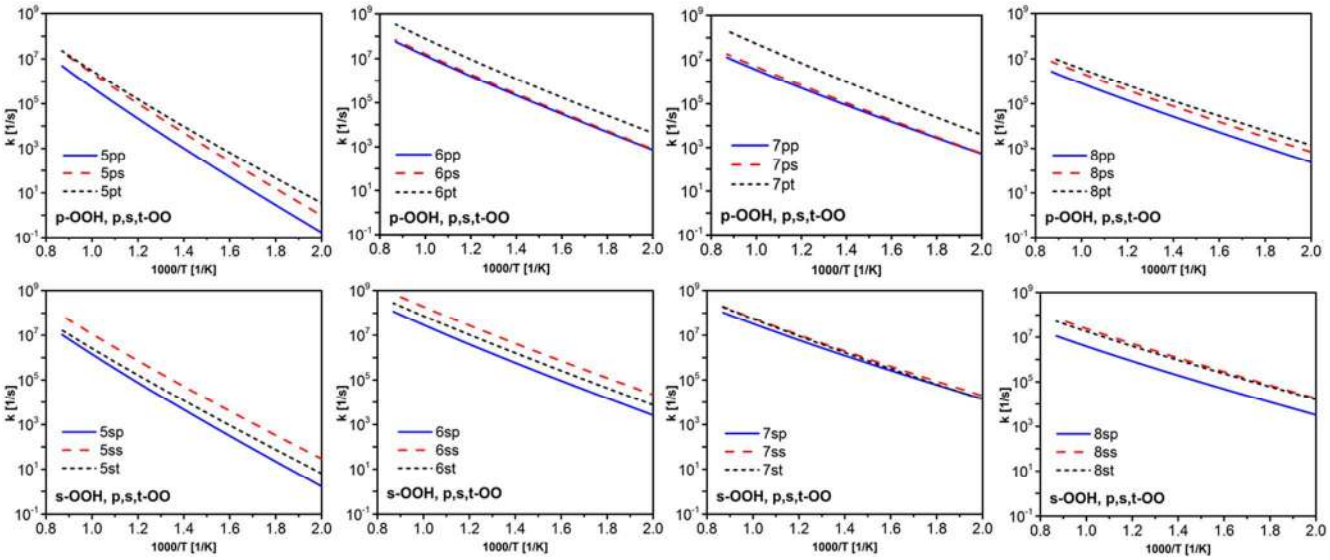

Figure 6. Effect of peroxy position on rate constants. The legend in each plot follows the N*CD* nomeclature, where N is the ring size, *C* and *D* are the type of the C-OOH and C-OO· respectively

3.3.4 Effect of chirality

Chirality was observed for both reactants and transition states. In this study, only N*SS* reactants have two chiral centers. Meanwhile, transition states of the investigated reactions have only one chiral (or pseudo-chiral) center, except for those of N*PS* and N*SS* species, which have two chiral (or pseudo-chiral) centers. For transition states with one chiral center, the two conformers (R or S) are mirror images.

To study the effect of chirality on kinetics, only the reactants and transition states with two chiral centers (N*PS* and N*SS)* are investigated. As mentioned earlier, the two conformers of the same chirality (RR and SS) are mirror images to each other, as are the two mixed (RS and RS) conformers. Therefore, only one conformer of each pair is considered and used to obtain the specific rate constants, as in Figure 7. For N*PS,* the differences in rates are merely a function of the energy difference between the mixed and same chirality conformers of transition states. The

energy difference (shown in Table 1) is below 1 kcal/mol for 1,4, 1,5 and 1,7 H-migrations while it is slightly higher (1.2 kcal/mol) for 1,6 H-migration. Therefore, in N*PS* the major difference in rates is observed for the 1,6 H-migration. On the other hand, for N*SS*, two chiral centers exist in the reactants and transition states. Thus, the rates are calculated for the mixed (or same) chirality using matching mixed (or same) chirality conformers in both the reactant and the transition states. This has resulted in a more pronounced effect of chirality on rate constants, which can be as much as an order of magnitude under atmospheric conditions, especially for 6*SS*.

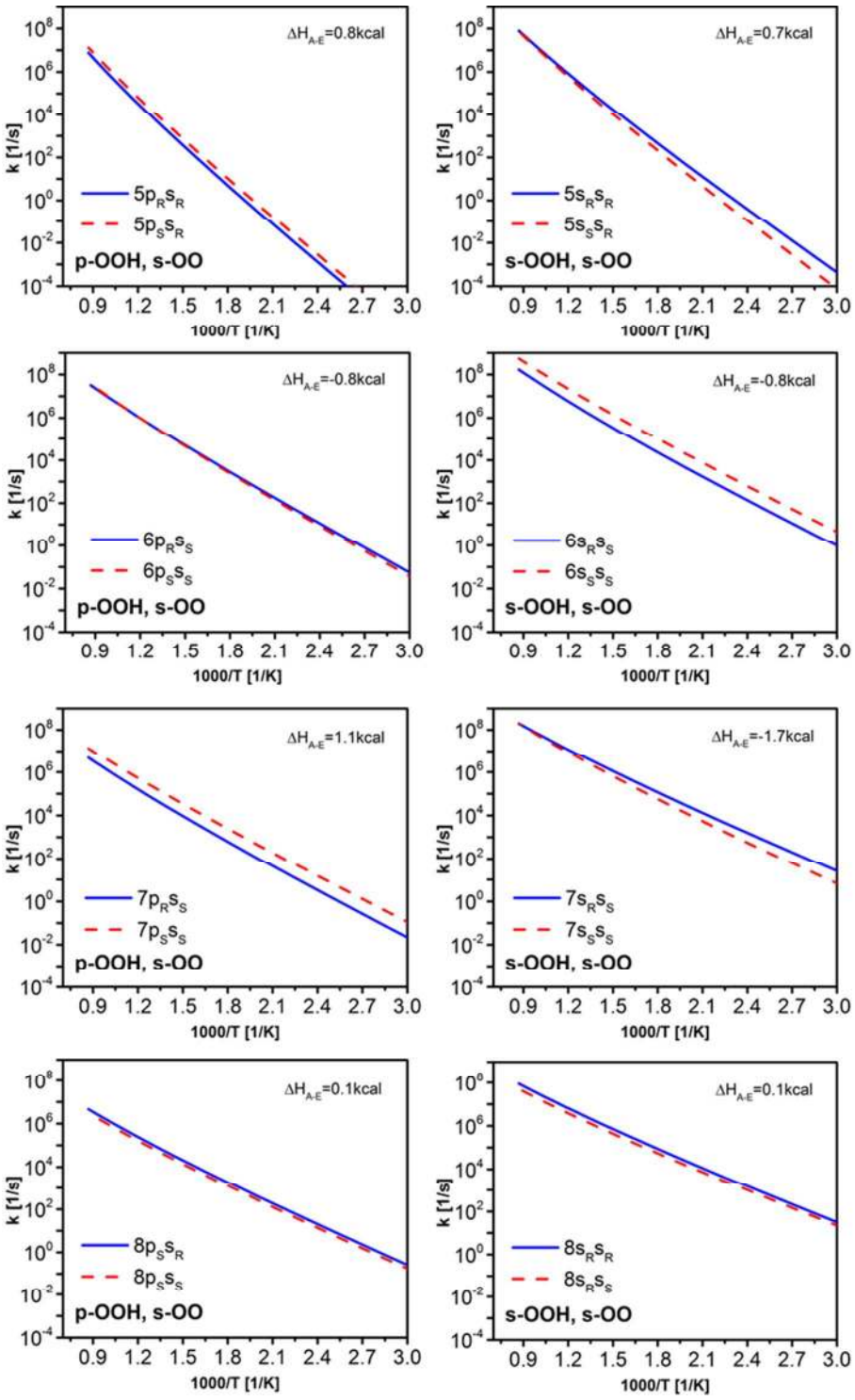

Figure 7. Effect of chirality on rate constants. The legend in each plot follows the N*CD* nomeclature, where N is the ring size, *C* and *D* correspond to the type of C-OOH and C-OO·, respectively. R and S subscripts indicate the chiral nature of the carbon.

3.4 Comparison with the literature

For the purpose of comparison to literature values, the rate constants calculated in this study for mixed and same chirality species and transition states are averaged. Our values are compared to those calculated at the CBS-QB3 [16-17] and modified CBS-QB3(MP2) [18] levels of theory.

General comparisons (Figure 8-11) show that better agreement is found for smaller ring size transition states than for larger ring sizes. This is due to larger systematic error associated with bigger molecules, especially when atomization reactions are used instead of isodesmic reactions. For the 1,4 H-migration, as shown in Figure 8, the calculated rates are in very good agreement with those of Sharma et al. [16] and Miyoshi [17], with discrepancies up to one order of magnitude at high temperatures in the case of the 5*PS* reaction. Disagreement at high temperatures is mainly due to the entropic effects resulting from the different HR treatment performed by Sharma et al. [16]. Yao et al. [18] reports site-specific rates for certain N*CD* reactions and an average rate rule intended for use in kinetic models. The site-specific rates reported by Yao et al. [18] are much faster (1 to 3 order of magnitude) than those calculated in this study, as well as those reported by Sharma et al. [16] and Miyoshi [17]. This may be attributed to the differences in activation energy resulting from the CBS-QB3(MP2) level of theory used for energy calculation. Yao et al. [18] suggested this method to optimize a di-hyrdoperoxidealkylradical $P(OOH)_2$, without considering the rapid decomposition to ketohydroperoxide and OH. Also, the enthalpy of formation was estimated using the atomization method. Discrepancies are also observed between A-factors calculated in this study and those reported by Yao et al. [18]. Such discrepancies are probably due to the fact that Yao et al. [18] did not calculate the energy barriers for all hindered rotors in the investigated species and transitions states. Instead, they calculated these barriers for representative rotors, and then used the same values for other rotors.

For the 1,5 H-migration, the calculated rates agree well with those of Miyoshi [17], but not with those reported by Sharma et al. [16] as shown in Figure 9. The discrepancy is seen at low temperatures, suggesting that tunneling may be the cause. Sharma et al. [16] use the Wigner method that underestimates tunneling corrections, leading to lower rates compared to those calculated by Miyoshi [17] and in this study where the Eckart tunneling method is adopted.

For the 1,6 H-migration (Figure 10), good agreement with Miyoshi [17] is observed, except for 7*PT,* 7*SS* and *7ST*. Similar slopes suggest that the major source of discrepancy is not the activation energy, but the entropic term. Miyoshi [17] did not calculate the hindered rotor barriers for all rotors. Instead, they used a representative rotational barrier for some rotors. Yao et al. [18] followed the same procedure which, along with the invalidated CBS-QB3(MP2) method used for the energy calculations, resulted in the notable discrepancy. Also for 1,6 H-migration, the rates reported by Sharma et al. [16] are close to an order of magnitude slower than the calculated rates, especially at high temperatures, which might be attributed to the entropic effects and the coupled hindered rotor treatment adopted by Sharma et al. [16]. Furthermore, the transition states considered by Sharma for the 1,6 H-migration reactions (eg. 7*PS*, 7*SP* and 7*SS*) are different than the most stable cyclohexane-like conformers determined this study. The greater ring strain of the transition states considered by Sharma results in higher barriers, and ultimately, slower rates compared to the ones obtained in this work.

The greatest discrepancy between the calculated rates and those available in the literature is observed for 1,7 H-migration site specific rates, except for 8*SP* and 8*PP,* where the calculated rate for the former is in very good agreement with those of Sharma et al. [16] and Miyoshi [17]. In the case of 8*PP,* the rates are in a good agreement with Miyoshi [17], while the disagreement with Sharma et al. [16] rates is mainly due to the entropic term (A factor), as evidenced by the identical

slopes observed in Figure 11 for this reaction. Meanwhile, the y-axis intercept obtained in this study is ten times greater than that obtained by Sharma et al. [16]. Compared to Yao et al. [18], our rates of 8*PP* are orders of magnitude slower. Again, the discrepancies are due to the fact that Yao et al. [18] did not consider HR treatment for each rotor, and Sharma et al. [16] used the coupled HR treatment. Also, Sharma's minimum energy conformer for the 8*PP* reactant is an HB structure, while the most stable conformer optimized in this work is an NHB structure. Optimizing Sharma's conformer with the same level of theory adopted in this study resulted in higher energy compared to the NHB conformer. For *8PS* and 8*SP*, the same difference is detected compared to Yao et al. [18], whereas the major difference compared to Miyoshi [17] is noticeable at low temperatures (below 715K). Although Miyoshi used the same Eckart tunneling as in this study, he fitted the rates to a two parameter Arrhenius model, which will not show the strong temperature dependence at low temperatures as found in this study.

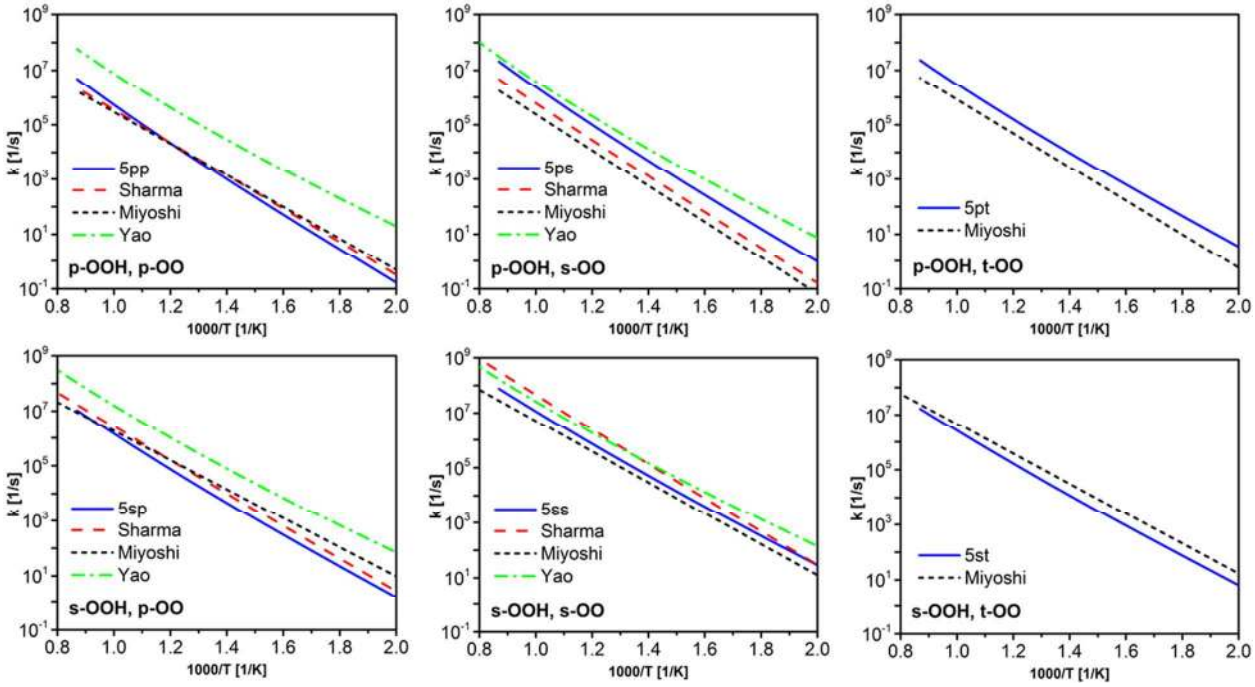

Figure 8. Calculated rates in this study for 1,4 H-migration (Blue solid lines) compared to literature values [16-18].

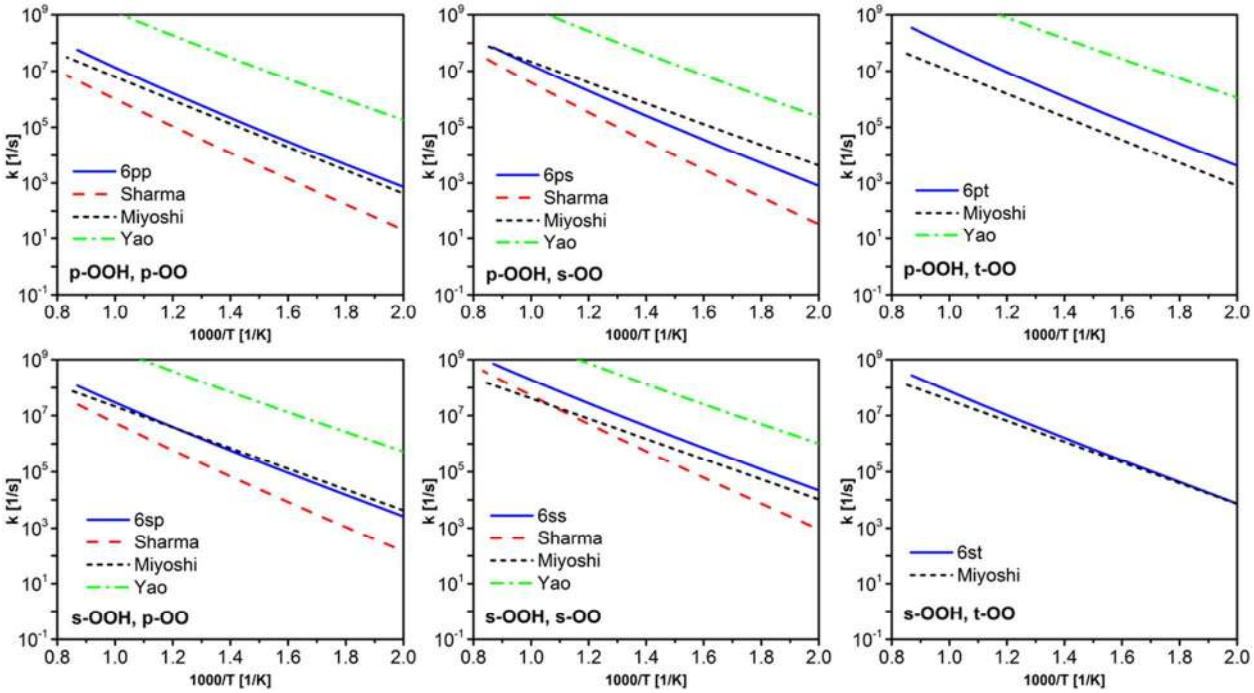

Figure 9. Calculated rates in this study for 1,5 H-migration (Blue solid lines) compared to literature values [16-18].

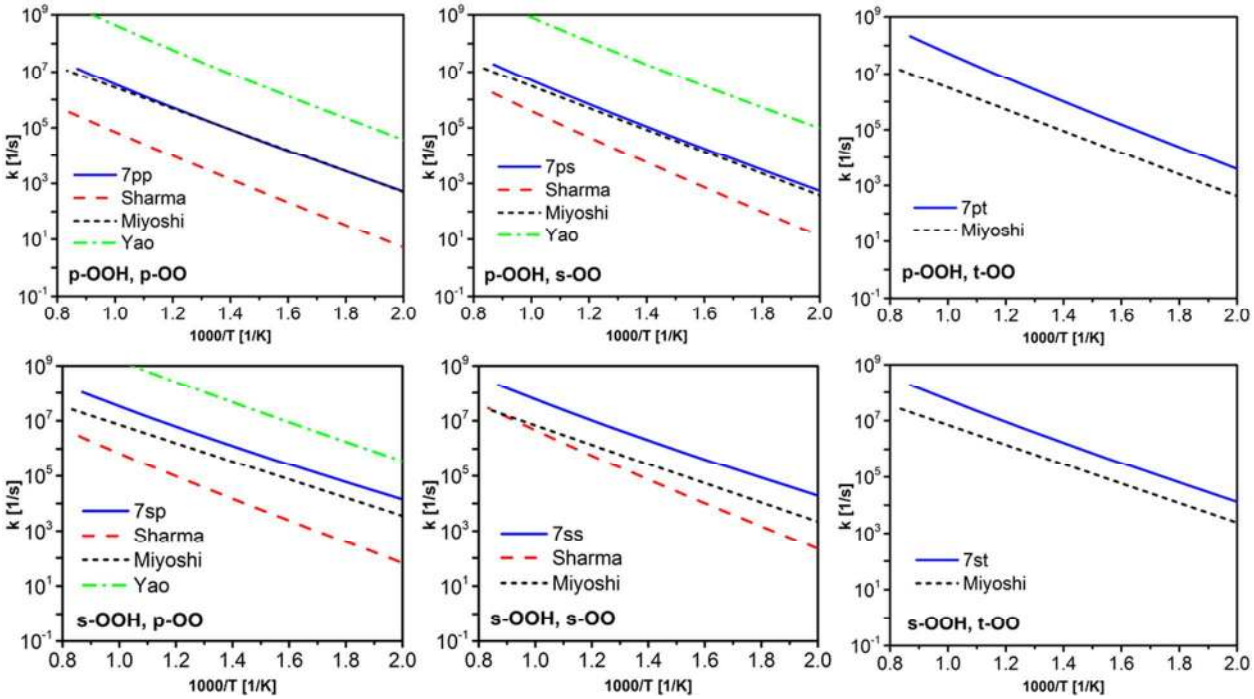

Figure 10. Calculated rates in this study for 1,6 H-migration (Blue solid lines) compared to literature values [16-18].

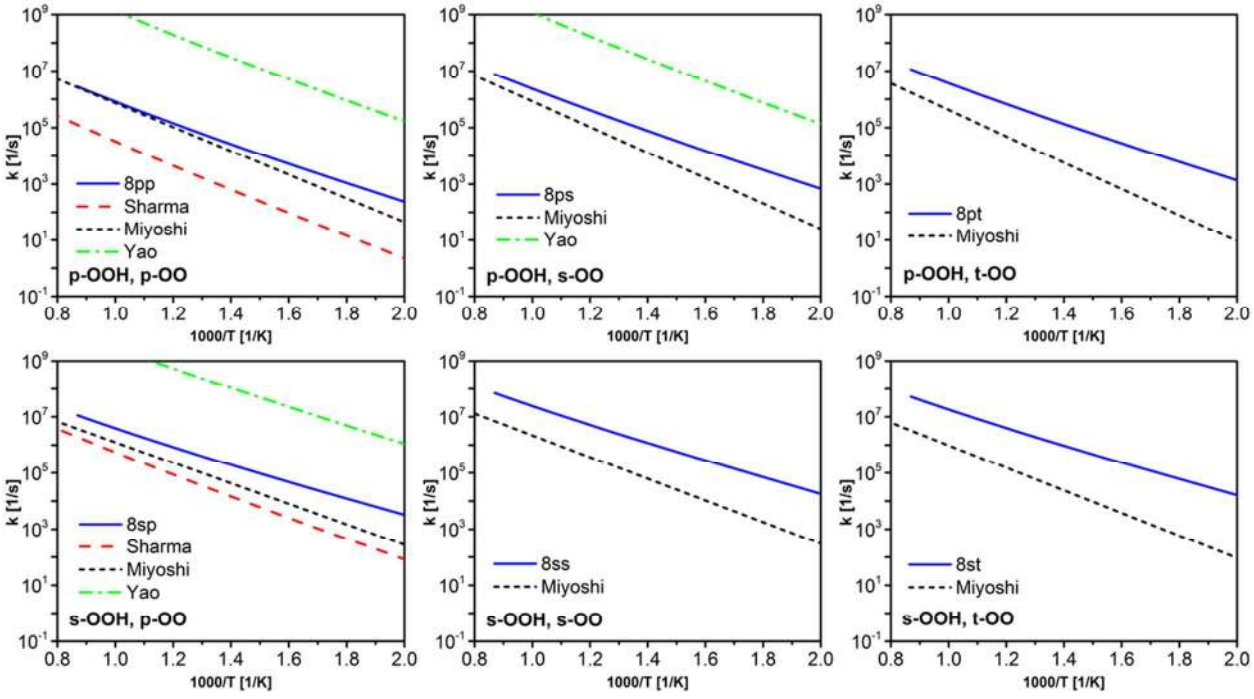

Figure 11. Calculated rates in this study for 1,7 H-migration (Blue solid lines) compared to literature values [16-18].

4. Implications for chemical kinetic modeling

To assess the implications of using the calculated rate constants in kinetic models, the site specific rate rules are implemented in models for 2-methylhexane [9] and iso-octane (2,2,4-trimethylpentane) [10], which originally used Sharma et al. [16] rates as estimates. Since Sharma et al. [16] did not provide all site specific rate rules, analogies were adopted for some rate rules in the original 2-methylhexane [9] model. Ignition delay times were simulated in a closed homogenous batch reactor model in Chemkin-Pro [48] software using the updated model. The ignition delay times were compared to the original model behavior at equivalence ratio of 1 and 0.5, 20 and 40 atm. At the investigated conditions, the effect of the calculated rate constants for OOQOOH isomerization reactions on ignition delay times of 2-methylhexane was found to be minor (Figure 12). The updated model predicts shorter ignition delay times at low temperatures below 800 K, which can be attributed to the rates calculated herein being faster than those from Sharma et al. [16]. In the case of iso-octane, the new rates notably increased the reactivity for iso-octane, as shown in Figure 13. Ignition delay times at 40 atm are shorter below 900 K. The rates calculated herein have a notable effect on iso-octane ignition delay times because six-membered ring OOQOOH isomerizations are the primary chain branching pathway; the faster rates calculated here have a significant effect on increasing low temperature reactivity. Additional detailed theoretical calculations are needed for alternative isomerization pathways to improve the kinetic modeling predictions of experimental data.

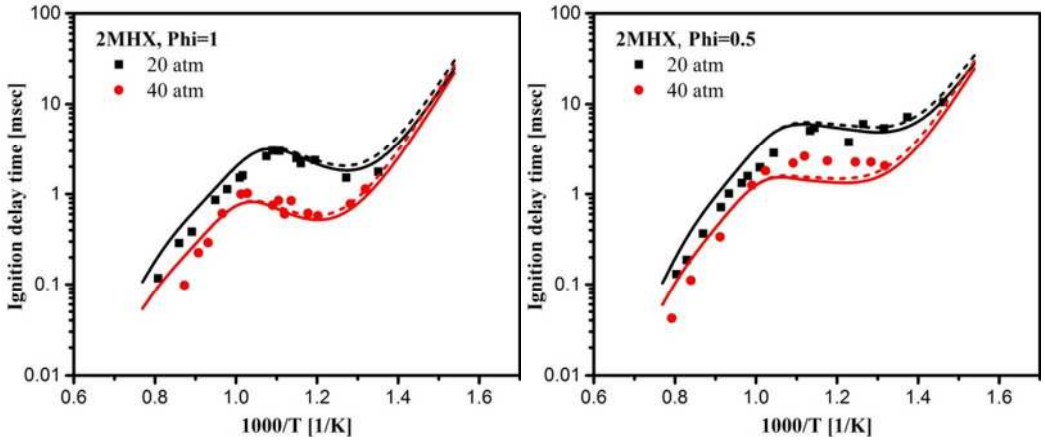

Figure 12. Ignition delay time of 2-methylhexane at ϕ=1 and 0.5, 20 and 40 atm against experimental data from Mohamed et al. [9]. Solid lines are the simulations using the rate rules for OOQOOH isomerization calculated in this work, compared to dashed lines using Sharma et al.[16] rates.

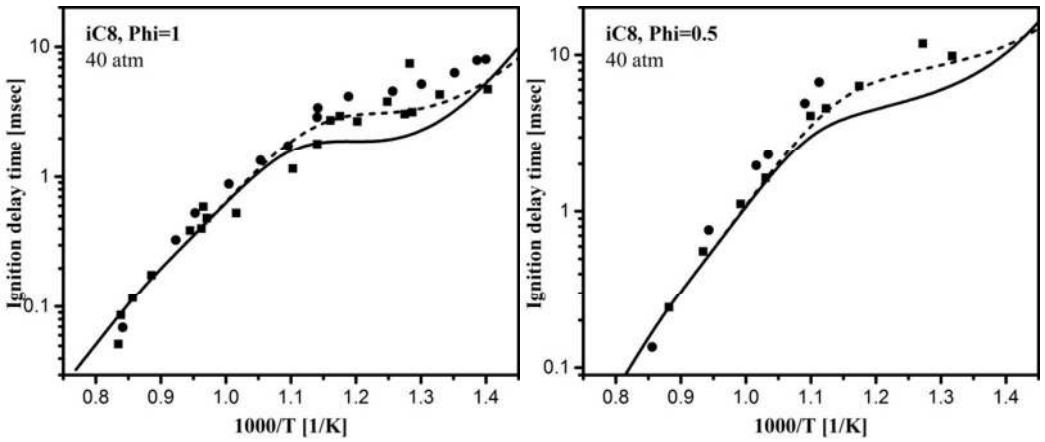

Figure 13. Ignition delay time of iso-octane at ϕ=1 and 0.5, 40 atm against experimental data from Fieweger et al. [49] (squares) and Hartmann et al. [50] (circles). Solid lines are the simulations using the rate rules for OOQOOH isomerization calculated in this work, compared to dashed lines using Sharma et al.[16] rates.

5. Summary and conclusion

In this work, the kinetics of OOQOOH radical isomerization is investigated and the rate parameters calculated. Five-, six-, seven- and eight-membered ring transition states, with different combinations of carbon site types for the hydroperoxide and peroxy groups are considered. The rate constants are calculated using classical transition state theory and fitted to a modified three-parameter Arrhenius equation over the temperature range of 300-1500K. Energy calculations were performed using CBS-QB3, G3 and G4 composite methods for minimum energy conformers. The minimum energy conformers were determined by considering all possible configurations of the reactants, products and transition states. 1D Hindered rotor treatment and Eckart tunneling were also considered.

A detailed conformational analysis was conducted to investigate the effect of chirality and HB on minimum energy conformers. It was found that, depending on the steric cost imposed by the HB ring, HB conformers were not always lower in energy (more stable). Chirality was considered for all chiral centers in the investigated molecules and transition states. For reactants with two chiral centers, conformers with mixed or the same chirality at both centers were considered. Meanwhile, transition state conformers wherein the substituents were in the axial or equatorial position were considered. Transition states with an axial configuration were found to be lower in energy when HB existed, but in some cases equatorial was preferred, especially when the axial configuration exhibited additional unfavorable gauche interactions. The effect of chirality on the kinetics was also discussed. Although two chiral conformers can be up to 3 kcal/mol different in energy, a very minor effect was observed on rate constants, especially under atmospheric conditions.

In terms of ring size, 1,5 H-migration was found to proceed via the same, or slightly higher, barrier than the 1,6 H-migration, as both transition state rings are cyclohexane-like. Since previous studies have not given much attention to rates where the peroxy group is in the tertiary site, the effect of the peroxy position was also discussed, and differences of up to an order of magnitude were observed. The calculated rates showed good agreement with the literature rates from Miyoshi [17]; however, some discrepancy is observed when compared to Sharma et al. [16] and Yao et al. [18]. This demonstrates the importance of the selected levels of theory for calculations, and the methods used to account for tunneling and entropic corrections. Finally, the calculated rates were shown to alter chemical kinetic modeling predictions of ignition delay time, especially in highly branched molecules where ignition is very sensitive to the KHP formation rate.

ASSOCIATED CONTENT

Supporting Information

(1) Tabulation of the calculated and isodesmic species energies at 298K using CBS-QB3, G3, G4. (2) Isodesmic reactions and the estimated enthalpy of formation for the calculated species. (3) Frequencies and Rotational constants for species and transition states (4) Cartesian coordinates for all reactants, transition states (both chiral conformers) and products. (5) Arrhenius parameters for reactions with two chiral centers (mixed and same chirality).

AUTHOR INFORMATION

Corresponding Author

*Email: davis.alexander.c@gmail.com

ACKNOWLEDGMENT

This work was supported by King Abdullah University of Science and Technology, Office of Sponsored Research (OSR) under Award OSR-2016-CRG5-3022, and Saudi Aramco under the FUELCOM program.

REFERENCES

1. Wang, Z.; Popolan-Vaida, D. M.; Chen, B.; Moshammer, K.; Mohamed, S. Y.; Wang, H.; Sioud, S.; Raji, M. A.; Kohse-Höinghaus, K.; Hansen, N.; Dagaut, P.; Leone, S. R.; Sarathy, S. M., Unraveling the Structure and Chemical Mechanisms of Highly Oxygenated Intermediates in Oxidation of Organic Compounds. *Proc. Natl. Acad. Sci. U.S.A.* **2017**.
2. Westbrook, C. K.; Pitz, W. J.; Curran, H. C.; Boercker, J.; Kunrath, E., Chemical Kinetic Modeling Study of Shock Tube Ignition of Heptane Isomers. *Int J Chem Kinet* **2001,** *33*, 868-877.
3. Zádor, J.; Taatjes, C. A.; Fernandes, R. X., Kinetics of Elementary Reactions in Low-Temperature Autoignition Chemistry. *Prog. Energy Combust. Sci.* **2011,** *37*, 371-421.
4. Merchant, S. S.; Goldsmith, C. F.; Vandeputte, A. G.; Burke, M. P.; Klippenstein, S. J.; Green, W. H., Understanding Low-Temperature First-Stage Ignition Delay: Propane. *Combust Flame* **2015,** *162*, 3658-3673.
5. Westbrook, C. K.; Pitz, W. J.; Herbinet, O.; Curran, H. J.; Silke, E. J., A Comprehensive Detailed Chemical Kinetic Reaction Mechanism for Combustion of N-Alkane Hydrocarbons from N-Octane to N-Hexadecane. *Combust Flame* **2009,** *156*, 181-199.
6. Cai, L.; Pitsch, H.; Mohamed, Y., Samah; Raman, V.; Bugler, J.; Curran, H. J.; Sarathy, S. M., Optimized Reaction Mechanism Rate Rules for Normal Alkanes. *Combust Flame* **2015**.
7. Sarathy, S. M.; Westbrook, C. K.; Mehl, M.; Pitz, W. J.; Togbe, C.; Dagaut, P.; Wang, H.; Oehlschlaeger, M. A.; Niemann, U.; Seshadri, K.; Veloo, P. S.; Ji, C.; Egolfopoulos, F. N.; Lu, T., Comprehensive Chemical Kinetic Modeling of the Oxidation of 2-Methylalkanes from C7 to C20. *Combust Flame* **2011,** *158*, 2338-2357.
8. Sarathy, S. M.; Javed, T.; Karsenty, F.; Heufer, A.; Wang, W.; Park, S.; Elwardany, A.; Farooq, A.; Westbrook, C. K.; Pitz, W. J.; Oehlschlaeger, M. A.; Dayma, G.; Curran, H. J.; Dagaut, P., A Comprehensive Combustion Chemistry Study of 2,5-Dimethylhexane. *Combust Flame* **2014,** *161*, 1444-1459.
9. Mohamed, S. Y.; Cai, L.; Khaled, F.; Banyon, C.; Wang, Z.; Al Rashidi, M. J.; Pitsch, H.; Curran, H. J.; Farooq, A.; Sarathy, S. M., Modeling Ignition of a Heptane Isomer: Improved Thermodynamics, Reaction Pathways, Kinetics, and Rate Rule Optimizations for 2-Methylhexane. *J Phys Chem A* **2016,** *120*, 2201-2217.
10. Atef, N.; Kukkadapu, G.; Mohamed, S. Y.; Rashidi, M. A.; Banyon, C.; Mehl, M.; Heufer, K. A.; Nasir, E. F.; Alfazazi, A.; Das, A. K.; Westbrook, C. K.; Pitz, W. J.; Lu, T.; Farooq, A.; Sung, C.-J.; Curran, H. J.; Sarathy, S. M., A Comprehensive Iso-Octane Combustion Model with Improved Thermochemistry and Chemical Kinetics. *Combust Flame* **2017,** *178*, 111-134.
11. Pitz, W. J.; Mueller, C. J., Recent Progress in the Development of Diesel Surrogate Fuels. *Prog. Energy Combust. Sci.* **2011,** *37*, 330-350.
12. Sarathy, S. M.; Farooq, A.; Kalghatgi, G. T., Recent Progress in Gasoline Surrogate Fuels. *Prog. Energy Combust. Sci.* **2018,** *65*, 67-108.
13. Al Rashidi, M. J.; Mehl, M.; Pitz, W. J.; Mohamed, S.; Sarathy, S. M., Cyclopentane Combustion Chemistry. Part I: Mechanism Development and Computational Kinetics. *Combust Flame* **2017,** *183*, 358-371.

14. Al Rashidi, M. J.; Mármol, J. C.; Banyon, C.; Sajid, M. B.; Mehl, M.; Pitz, W. J.; Mohamed, S.; Alfazazi, A.; Lu, T.; Curran, H. J.; Farooq, A.; Sarathy, S. M., Cyclopentane Combustion. Part Ii. Ignition Delay Measurements and Mechanism Validation. *Combust Flame* **2017,** *183*, 372-385.
15. Battin-Leclerc, F., Detailed Chemical Kinetic Models for the Low-Temperature Combustion of Hydrocarbons with Application to Gasoline and Diesel Fuel Surrogates. *Prog. Energy Combust. Sci.* **2008,** *34*, 440-498.
16. Sharma, S.; Raman, S.; Green, W. H., Intramolecular Hydrogen Migration in Alkylperoxy and Hydroperoxyalkylperoxy Radicals: Accurate Treatment of Hindered Rotors. *J Phys Chem A* **2010,** *114*, 5689-5701.
17. Miyoshi, A., Systematic Computational Study on the Unimolecular Reactions of Alkylperoxy (Ro2), Hydroperoxyalkyl (Qooh), and Hydroperoxyalkylperoxy (O2qooh) Radicals. *J Phys Chem A* **2011,** *115*, 3301-25.
18. Yao, Q.; Sun, X.-H.; Li, Z.-R.; Chen, F.-F.; Li, X.-Y., Pressure-Dependent Rate Rules for Intramolecular H-Migration Reactions of Hydroperoxyalkylperoxy Radicals in Low Temperature. *J Phys Chem A* **2017,** *121*, 3001-3018.
19. Goldsmith, C. F.; Green, W. H.; Klippenstein, S. J., Role of O2 + Qooh in Low-Temperature Ignition of Propane. 1. Temperature and Pressure Dependent Rate Coefficients. *J Phys Chem A* **2012,** *116*, 3325-46.
20. Asatryan, R.; Bozzelli, J. W., Chain Branching and Termination in the Low-Temperature Combustion of N-Alkanes: 2-Pentyl Radical + O2, Isomerization and Association of the Second O2. *J Phys Chem A* **2010,** *114*, 7693-7708.
21. Wang, Z.; Zhang, L.; Moshammer, K.; Popolan-Vaida, D. M.; Shankar, V. S. B.; Lucassen, A.; Hemken, C.; Taatjes, C. A.; Leone, S. R.; Kohse-Höinghaus, K.; Hansen, N.; Dagaut, P.; Sarathy, S. M., Additional Chain-Branching Pathways in the Low-Temperature Oxidation of Branched Alkanes. *Combust Flame* **2016,** *164*, 386-396.
22. Wang, Z.; Sarathy, S. M., Third O2 Addition Reactions Promote the Low-Temperature Auto-Ignition of N-Alkanes. *Combust Flame* **2016,** *165*, 364-372.
23. Wang, Z.; Mohamed, S. Y.; Zhang, L.; Moshammer, K.; Popolan-Vaida, D. M.; Shankar, V. S. B.; Lucassen, A.; Ruwe, L.; Hansen, N.; Dagaut, P.; Sarathy, S. M., New Insights into the Low-Temperature Oxidation of 2-Methylhexane. *Proc Combust Inst* **2017,** *36*, 373-382.
24. Wang, Z.; Chen, B.; Moshammer, K.; Popolan-Vaida, D. M.; Sioud, S.; Shankar, V. S. B.; Vuilleumier, D.; Tao, T.; Ruwe, L.; Bräuer, E.; Hansen, N.; Dagaut, P.; Kohse-Höinghaus, K.; Raji, M. A.; Sarathy, S. M., N-Heptane Cool Flame Chemistry: Unraveling Intermediate Species Measured in a Stirred Reactor and Motored Engine. *Combust Flame* **2018,** *187*, 199-216.
25. Curran, H. J.; Gaffuri, P.; Pitz, W. J.; Westbrook, C. K., A Comprehensive Modeling Study of N-Heptane Oxidation. *Combust Flame* **1998,** *114*, 149-177.
26. Curran, H. J.; Gaffuri, P.; Pitz, W. J.; Westbrook, C. K., A Comprehensive Modeling Study of Iso-Octane Oxidation. *Combust Flame* **2002,** *129*, 253-280.
27. Bugler, J.; Somers, K. P.; Silke, E. J.; Curran, H. J., Revisiting the Kinetics and Thermodynamics of the Low-Temperature Oxidation Pathways of Alkanes: A Case Study of the Three Pentane Isomers. *J Phys Chem A* **2015,** *119*, 7510-7527.
28. Davis, A. C.; Francisco, J. S., Hydroxyalkoxy Radicals: Importance of Intramolecular Hydrogen Bonding on Chain Branching Reactions in the Combustion and Atmospheric Decomposition of Hydrocarbons. *J Phys Chem A* **2014,** *118*, 10982-11001.
29. Davis, A. C.; Francisco, J. S., Ab Initio Study of Key Branching Reactions in Biodiesel and Fischer–Tropsch Fuels. *J Am Chem Soc* **2011,** *133*, 19110-19124.

30. Davis, A. C.; Francisco, J. S., Ab Initio Study of Hydrogen Migration across N-Alkyl Radicals. *J Phys Chem A* **2011,** *115*, 2966-2977.
31. Frisch, M. J.; Trucks, G. W.; Schlegel, H. B.; Scuseria, G. E.; Robb, M. A.; Cheeseman, J. R.; Scalmani, G.; Barone, V.; Mennucci, B.; Petersson, G. A. et al. *Gaussian 09*, Gaussian, Inc.: Wallingford, CT, USA, 2009.
32. Andersson, M. P.; Uvdal, P., New Scale Factors for Harmonic Vibrational Frequencies Using the B3lyp Density Functional Method with the Triple-Z Basis Set 6-311+G(D,P). *J Phys Chem A* **2005,** *109*, 2937-2941.
33. Jr., J. A. M.; Frisch, M. J.; Ochterski, J. W.; Petersson, G. A., A Complete Basis Set Model Chemistry. Vii. Use of the Minimum Population Localization Method. *J Chem Phys* **2000,** *112*, 6532-6542.
34. Curtiss, L. A.; Raghavachari, K.; Redfern, P. C.; Rassolov, V.; Pople, J. A., Gaussian-3 (G3) Theory for Molecules Containing First and Second-Row Atoms. *J Chem Phys* **1998,** *109*, 7764-7776.
35. Curtiss, L. A.; Redfern, P. C.; Raghavachari, K., Gaussian-4 Theory Using Reduced Order Perturbation Theory. *J Chem Phys* **2007,** *127*, 124105.
36. Hehre, W. J.; Ditchfield, R.; Radom, L.; Pople, J. A., Molecular Orbital Theory of the Electronic Structure of Organic Compounds. V. Molecular Theory of Bond Separation. *J Am Chem Soc* **1970,** *92*, 4796-4801.
37. Karton, A.; Gruzman, D.; Martin, J. M. L., Benchmark Thermochemistry of the Cnh2n+2 Alkane Isomers (N = 2−8) and Performance of Dft and Composite Ab Initio Methods for Dispersion-Driven Isomeric Equilibria. *J Phys Chem A* **2009,** *113*, 8434-8447.
38. Wheeler, S. E.; Houk, K. N.; Schleyer, P. v. R.; Allen, W. D., A Hierarchy of Homodesmotic Reactions for Thermochemistry. *J Am Chem Soc* **2009,** *131*, 2547-2560.
39. Ruscic, B.; Bross, D. H., *Active Thermochemical Tables (Atct) Values Based on Ver. 1.122 of the Thermochemical Network* 2016.
40. Linstrom, P. J.; Mallard, W. G., *Nist Chemistry Webbook, Nist Standard Reference Database Number 69*. National Institute of Standards and Technology: Gaithersburg MD.
41. Somers, K. P.; Simmie, J. M., Benchmarking Compound Methods (Cbs-Qb3, Cbs-Apno, G3, G4, W1bd) against the Active Thermochemical Tables: Formation Enthalpies of Radicals. *J Phys Chem A* **2015,** *119*, 8922-8933.
42. Pitzer, K. S., Energy Levels and Thermodynamic Functions for Molecules with Internal Rotation: Ii. Unsymmetrical Tops Attached to a Rigid Frame. *J Chem Phys* **1946,** *14*, 239-243.
43. Bao, J. L.; Truhlar, D. G., Variational Transition State Theory: Theoretical Framework and Recent Developments. *Chem. Soc. Rev.* **2017,** *46*, 7548-7596.
44. ALLISON, T. C.; TRUHLAR, D. G., Testing the Accuracy of Practical Semiclassical Methods: Variational Transition State Theory with Optimized Multidimensional Tunneling. In *Modern Methods for Multidimensional Dynamics Computations in Chemistry*, WORLD SCIENTIFIC: 2011; pp 618-712.
45. Cramer, C. J., *Essentials of Computational Chemistry: Theories and Models*. John Wiley & Sons: 2013.
46. Mokrushin, V.; Bedanov, V.; Tsang, W.; Zachariah, M.; Knyazev, V.; McGivern, W. *Chemrate, Version 1.5. 8*, Gaithersburg, MD, 2009.
47. Vereecken, L.; Peeters, J., Theoretical Investigation of the Role of Intramolecular Hydrogen Bonding in B-Hydroxyethoxy and B-Hydroxyethylperoxy Radicals in the Tropospheric Oxidation of Ethene. *J Phys Chem A* **1999,** *103*, 1768-1775.
48. *Chemkin-Pro 15112*, San Diego, 2012.
49. Fieweger, K.; Blumenthal, R.; Adomeit, G., Self-Ignition of S.I. Engine Model Fuels: A Shock Tube Investigation at High Pressure. *Combust Flame* **1997,** *109*, 599-619.

50. Hartmann, M.; Gushterova, I.; Fikri, M.; Schulz, C.; Schießl, R.; Maas, U., Auto-Ignition of Toluene-Doped N-Heptane and Iso-Octane/Air Mixtures: High-Pressure Shock-Tube Experiments and Kinetics Modeling. *Combust Flame* **2011,** *158*, 172-178.

Table of Contents Graphic: